Acta Oceanol. Sin., 2021, Vol. 40, No. 7, P. 183–197
https://doi.org/10.1007/s13131-021-1721-6
http://www.aosocean.com
E-mail: ocean2@hyxb.org.cn

Multi-beam and seismic investigations of the active Haima cold seeps, northwestern South China Sea

Bin Liu[1], Jiangxin Chen[2, 3]*, Li Yang[1], Minliang Duan[2, 4], Shengxuan Liu[1], Yongxian Guan[1], Pengcheng Shu[4]

[1] Key Laboratory of Marine Mineral Resources, Guangzhou Marine Geological Survey, Ministry of Natural Resources, Guangzhou 510760, China

[2] Key Laboratory of Gas Hydrate, Qingdao Institute of Marine Geology, Ministry of Natural Resources, Qingdao 266071, China

[3] Laboratory for Marine Mineral Resources, Pilot National Laboratory for Marine Science and Technology (Qingdao), Qingdao 266071, China

[4] Key Laboratory of Submarine Geosciences and Prospecting Techniques of Ministry of Education, Ocean University of China, Qingdao 266100, China

Received 10 October 2020; accepted 11 December 2020

Abstract

To confirm the seabed fluid flow at the Haima cold seeps, an integrated study of multi-beam and seismic data reveals the morphology and fate of four bubble plumes and investigates the detailed subsurface structure of the active seepage area. The shapes of bubble plumes are not constant and influenced by the northeastward bottom currents, but the water depth where these bubble plumes disappear (630–650 m below the sea level) (mbsl) is very close to the upper limit of the gas hydrate stability zone in the water column (620 m below the sea level), as calculated from the CTD data within the study area, supporting the "hydrate skin" hypothesis. Gas chimneys directly below the bottom simulating reflectors, found at most sites, are speculated as essential pathways for both thermogenic gas and biogenic gas migrating from deep formations to the gas hydrate stability zone. The fracture network on the top of the basement uplift may be heavily gas-charged, which accounts for the chimney with several kilometers in diameter (beneath Plumes B and C). The much smaller gas chimney (beneath Plume D) may stem from gas saturated localized strong permeability zone. High-resolution seismic profiles reveal pipe-like structures, characterized by stacked localized amplitude anomalies, just beneath all the plumes, which act as the fluid conduits conveying gas from the gas hydrate-bearing sediments to the seafloor, feeding the gas plumes. The differences between these pipe-like structures indicate the dynamic process of gas seepage, which may be controlled by the build-up and dissipation of pore pressure. The 3D seismic data show high saturated gas hydrates with high RMS amplitude tend to cluster on the periphery of the gas chimney. Understanding the fluid migration and hydrate accumulation pattern of the Haima cold seeps can aid in the further exploration and study on the dynamic gas hydrate system in the South China Sea.

Key words: fluid escape, cold seep, natural gas hydrate, bubble plume, Qiongdongnan Basin, South China Sea

Citation: Liu Bin, Chen Jiangxin, Yang Li, Duan Minliang, Liu Shengxuan, Guan Yongxian, Shu Pengcheng. 2021. Multi-beam and seismic investigations of the active Haima cold seeps, northwestern South China Sea. Acta Oceanologica Sinica, 40(7): 183–197, doi: 10.1007/s13131-021-1721-6

1 Introduction

Cold seeps are areas where gases and fluids leak into the ocean water column from the seafloor sediments (Judd and Hovland, 2007; Foucher et al., 2009). The word "cold" is used to distinguish them from the hydrothermal vents. Unlike hydrothermal vents that mostly occur near the ocean ridges where a new crust is formed or derived from magmatism in the sedimentary basins, cold seeps are widespread globally (Judd and Hovland, 2007). Cold seeps have attracted considerable attention because of their potential role in the global methane budget (Judd, 2003; Etiope, 2012) and their association with natural gas hydrates and seafloor ecosystems (Foucher et al., 2009; Suess, 2014).

The cold seeps can be verified by the presence of gas bubble plumes that can be detected using high-frequency acoustic methods. Gas bubble plumes often manifest themselves as gas flares in acoustic images that have been observed in most of the oceans around the world, such as the Hydrate Ridge (Bangs et al., 2011), Barbados (Barnard et al., 2015), Costa Rica (Crutchley et al., 2014), Hikurangi margin (Klaucke et al., 2010), Gulf of Mexico (Solomon et al., 2009), Mediterranean (Prinzhofer and Deville, 2013), Black Sea (Greinert et al., 2006), U.S. Atlantic margin (Brothers et al., 2013, 2014; Skarke et al., 2014), sub-Antarctic island (Römer et al., 2014) and the Svalbard continental margin (Westbrook et al., 2009).

Foundation item: The Shandong Province "Taishan Scholar" Construction Project; the fund of the Laboratory for Marine Mineral Resources, Pilot National Laboratory for Marine Science and Technology (Qingdao) under contract No. MMRKF201810; the National Natural Science Foundation of China under contract No. 41606077; the National Key R&D Program of China under contract No. 2018YFC0310000.

*Corresponding author, E-mail: jiangxin_chen@sina.com

In the South China Sea (SCS), numerous cold seeps have been discovered since the discovery of the "Jiu Long Methane Reef" in 2004 (Chen et al., 2005; Han et al., 2008). Cold seep-related seafloor features, e.g., mud volcanoes, gas seepages and pockmarks, have been identified in the Taixinan Basin (TXNB) (Chen et al., 2014), the Zhujiang River Mouth Basin (ZRMB) (Sun et al., 2012), the Yinggehai Basin (YGHB) (Huang et al., 2009), the Qiongdongnan Basin (QDNB) (Wang et al., 2018a; Zhang et al., 2019) and the Zhongjiannan Basin (ZJNB) (Chen et al., 2015a, b, 2018). An overview of the discovered cold seep systems in the SCS from the aspects of seabed manifestation, geochemical indicators and ecology system has been summarized (Feng et al., 2018). Most of the cold seeps in the northern SCS margin are currently inactive, at least since 11.5 ka BP (Tong et al., 2013; Han et al., 2014). Only two active cold-seep sites have been reported, which are Site F in the Dongsha area (Zhang et al., 2017) and the Haima cold seeps discovered during the dives of the Remote Operated Vehicle (ROV) "Haima" (Liang et al., 2017). Numerous geochemical studies on the Haima cold seeps have been conducted (Liang et al., 2017; Guan et al., 2018; Wang et al., 2018a; Feng et al., 2019; Hu et al., 2019; Fang et al., 2019), however, the geophysical and geological studies of this active seepage are limited. One 2D seismic line across Site ROV1 and Site ROV2 described the subsurface structures beneath the Haima cold seeps (Wang et al., 2018b). They thought magmatic activities probably make a big contribution to the Haima cold seeps (Wang et al., 2018b), which means that the Haima cold seeps may represent a unique active cold seep and natural gas hydrate system in the SCS (Liu and Liu, 2017; Yang et al., 2018), till now. Seismic data and samples geochemical analysis show that magmatism in the QDNB and Xisha massif was active during Middle Miocene and Pliocene (Zhao et al., 2016; Wang et al., 2019). Liang et al. (2017) and Wei et al. (2020) have given evidence of the existence of long-term gas venting (several thousands of years) at the Haima cold seeps, however, whether the Haima cold seeps were active over the Neogene is still unknown. More geophysical data and geological analysis should be conducted to study the subsurface structures beneath gas bubble plumes.

More recently, a systematic study based on the seafloor observation data and seismic data has been conducted, which presents a broader cold seep ecosystem and a potential fluid migration mechanism (Wei et al., 2020). However, the detailed subsurface structure and gas hydrate accumulation mechanism responsible for this active seepage environment, as well as the characteristic of gas plumes are still unclear. Therefore, the aims of this work are: (1) to study the behaviors of gas bubble plumes within the water column, the associated features on the seafloor and the subsurface structures using multi-beam and seismic data, (2) to characterize the fluid escape pathways and natural gas hydrate formation using high-resolution 3D seismic dataset and 2D seismic lines, and (3) to analyze and gain new insights to the unique fluid escape system. Our study may help to better understand the fluid flow and gas hydrate accumulation at the Haima cold seeps, having an implication for further gas hydrate research and exploration in the SCS.

2 Geological background and fluid flow system

The study area is located in the southwest of the QDNB, northwestern SCS, and neighbors Hainan Island to the north (Fig. 1a). The QDNB is a NE-trended Cenozoic sedimentary basin. Its evolution is closely related to the opening of the SCS (Yuan et al., 2009; Huang et al., 2016). This basin has experienced two-phase evolution, the rifting stage during Palaeogene and the post-rifting thermal subsidence stage since Neogene (Ru and Pigott, 1986; Lüdmann and Wong, 1999; Hu et al., 2013). The QDNB can be divided into five main tectonic zones: the northern depression belt, northern (central) uplift belt, central depression belt, southern depression belt, and southern uplift belt (Shi et al., 2013). Average rates of accumulation in QDNB are fluctuating and extremely high, i.e., 86 m/Ma in 45–36 Ma, 200–300 m/Ma in 36–15.5 Ma, 90–130 m/Ma in 15.5–5.5 Ma and 150–630 m/Ma since 5.5 Ma (Zhao et al., 2015). The rapid sedimentation rates cause overpressure and lead under-compaction at depths of greater than 3 300 m beneath the sea surface throughout the central QDNB, especially in deep water areas (Zhu et al., 2009; Huang et al., 2016). In addition, gas hydrate occurrence in the QDNB has been confirmed by the hydrate samples recovered at the Haima cold seeps and during the fifth gas hydrate drilling expedition conducted by the Guangzhou Marine Geological Survey (Liang et al., 2017; Wei et al., 2019; Ye et al., 2019; Liang et al., 2019). The Haima cold seeps lie in the Lingnan low uplift, belonging to the southern uplift belt (Fig. 1b). The present-day geothermal regime of the Haima cold seeps is characterized by a high heat flow (~85–105 mW/m^2; Shi et al., 2017).

Many cold seep-related seafloor features in the SCS have been reported, including mud volcanoes, pockmarks, and pipes (Bai et al., 2014; Chen et al., 2015a). During the dives of the ROV "Haima" in 2015, an active cold seep area was surprisingly discovered (Liang et al., 2017). Massive gas hydrates were recovered at Sites ROV1 and ROV2 (Fig. 1c). The oxygen isotopic results indicate probable destabilization of gas hydrates in the past and the carbon isotopic ages suggest a major episodic of carbonate precipitation between 6.1 ka and 5.1 ka BP (Liang et al., 2017). Moreover, dead bivalves are common at both Site ROV1 and Site ROV2 , suggesting a decline of seepage activity in recent time. The variation of seepage intensities is also indicated by lipid biomarker analysis (Guan et al., 2018) and the compositions of sediments (Wang et al., 2018a). Pore fluid analysis showed lateral migration of methane-rich fluids from the Site ROV1 to the nearby sites (QDN-14A and QDN-14B) which contributes to the enhanced methane flux at the nearby sites (Hu et al., 2019). The geochemical analysis finds that the gas hydrate samples from the Haima cold seeps are typical structure I hydrates and all the hydrate-bound gases are mixtures of biogenic and thermogenic gas (Fang et al., 2019). Moreover, in the latest study, three new gas plumes are discovered and a year-level spatiotemporal variation of cold seeps is confirmed by comparing different multibeam datasets obtained in 2016 and 2018 (Wei et al., 2020).

3 Datasets and methods

Multi-beam data comprise bathymetric, backscatter and water column data that were acquired in 2016 with a Kongsberg EM122 system, operating at 11.25–12.60 kHz. The water column data and depth data were simultaneously recorded in a grid pattern with an acquisition line spacing of 700 m. The speed of the vessel was about 4 m/s, and the interval of shooting was ca. 2.5 s. The raw data are processed in the Caris HIPS and SIPS 8.1 software by the following sequence: navigation filtering, parameters calibration, correction for transducer draft, correction for sound velocity, data filtering and interpolation. The cell size of the raster grids is 20 m×20 m and the vertical resolution is ca. 3‰ of the water depth. Water column images capturing the bubble plumes from the Haima cold seeps are derived from the same software.

A 3D seismic survey was conducted by the Guangzhou Marine Geological Survey (GMGS) to assess the potential of gas hydrates in the cold seep area, in 2013. The 3D seismic survey is

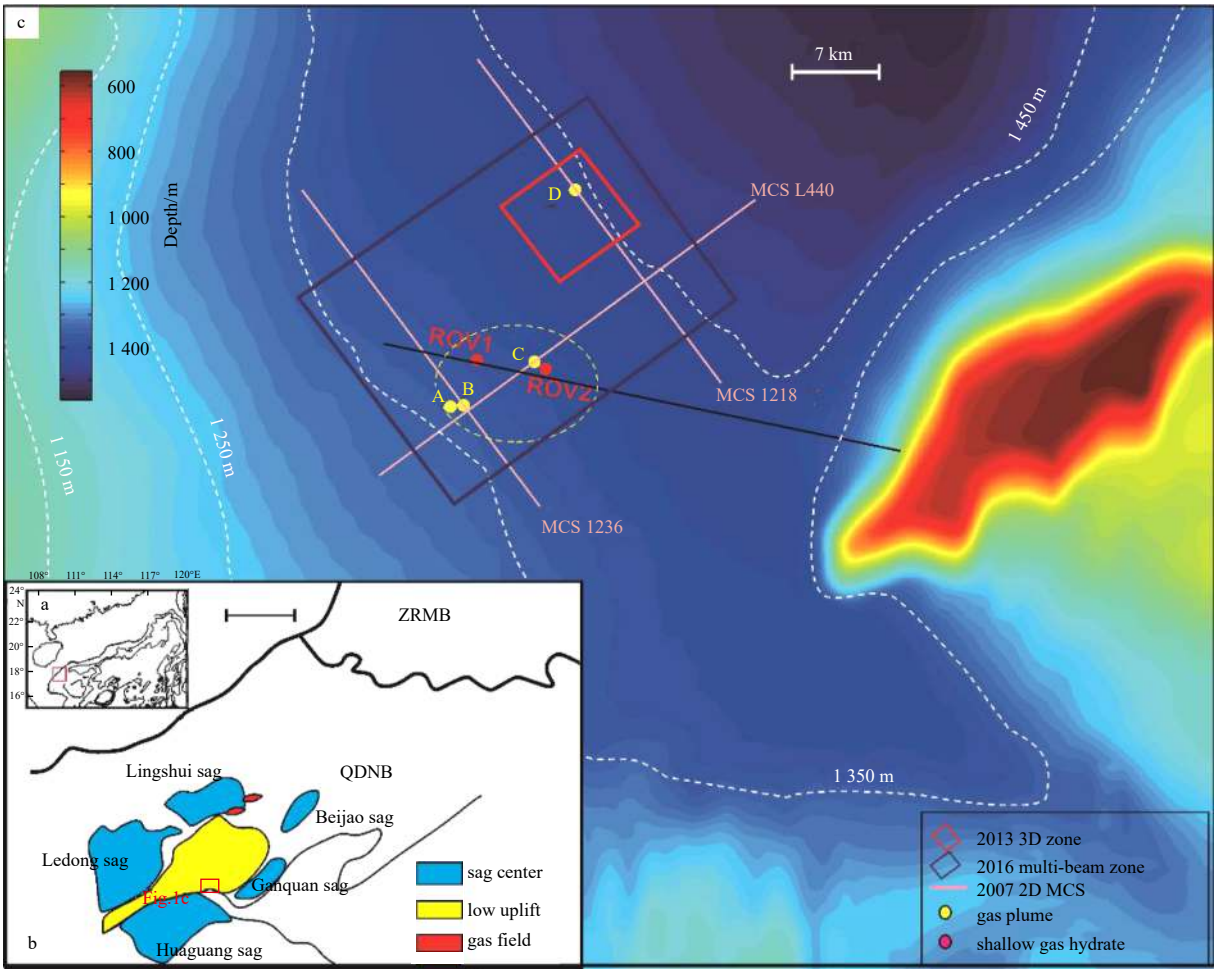

Fig. 1. Location of the geological map on the northern slope of SCS (a); geological background of the Haima cold seeps, and the study area is surrounded by several sags (b); and four sites of gas bubble plumes (yellow circle), labeled as A, B, C, and D were observed in the multi-beam water-column data (c). The pink lines are 2D multichannel seismic lines that pass through the plumes. Note that Plumes B, C, and D are crossed by seismic lines Multi-Channel Seismic (MCS) 1236, MCS L440, MCS 1218, respectively. Near-seafloor gas hydrates were recovered at Sites ROV1 and ROV2 (red dots) at 3–8 m below the seafloor with a 9 m-long, 73 cm-wide, and 1 000 kg-weight gravity piston corer (PC). The black line through ROV1 and ROV2 is the seismic line shown in Wang et al. (2018b). ZRMB: Zhujiang River Mouth Basin, QDNB: Qiongdongnan Basin.

achieved by acquiring densely-spaced 2D lines and processing them with 3D method. The shot line spacing is 100 m and the shot spacing is 12.5 m. The streamer has 768 channels and the interval is 3.125 m. The 3D seismic dataset was processed on the basis of standard industry protocol. The data were high-pass filtered with the low-frequency limit of 3–6 Hz. A frequency-dependent method was used to attenuate the noise, and the multiples were attenuated in a 3D way. The bin size is 3.125 m×50 m. The routine normal moveout (NMO) velocity analysis was used to produce the velocity model. Finally, the 3D prestack Kirchhoff time migration was used to obtain the images of subsurface structures.

The high-resolution multichannel seismic (MCS) data were acquired by GMGS in 2007 with the aim to investigate the nature and distribution of gas hydrates. The seismic source is a GI gun array with a total volume of 160 cu.in (1 cu.in=16.387 cm^3). The shot spacing is 25 m. A streamer of 240 channels with a spacing of 12.5 m was used to record the seismic data. This dataset has been processed commercially, and the post-stack migration method was used to obtain the subsurface image. Data were high-pass filtered with the low-frequency limit of 10 Hz. The FK filter method was used to attenuate the strong linear noise. The multiples were attenuated by jointly applying the high-resolution radon transform and the near-offset trace muting. The velocity model was produced based on the routine normal move-out (NMO) velocity analysis. Finally, the prestack Kirchhoff time migration was used to obtain the images of the subsurface structure. The final migration data has a frequency band of 10–120 Hz and a dominant frequency of ~60 Hz. The vertical resolution of the data is about 6.25 m in the shallow part, the velocity provided is 1 500 m/s and the vertical resolution is 1/4 wavelength.

4 Results

4.1 *Surface expressions of the Haima cold seeps*

The Haima cold seeps are discovered in 2015 and cover a wide area (over 400 km^2) in the central QDNB. Based on newly acquired multibeam bathymetry data, four massive gas venting plumes, named A, B, C, and D (in order of their discovery time), are confirmed in the water column images (Fig. 2). Gas bubbles were observed to tilt up in the same direction, manifesting themselves as flares. These plumes are 735 m, 750 m, 770 m, and 823

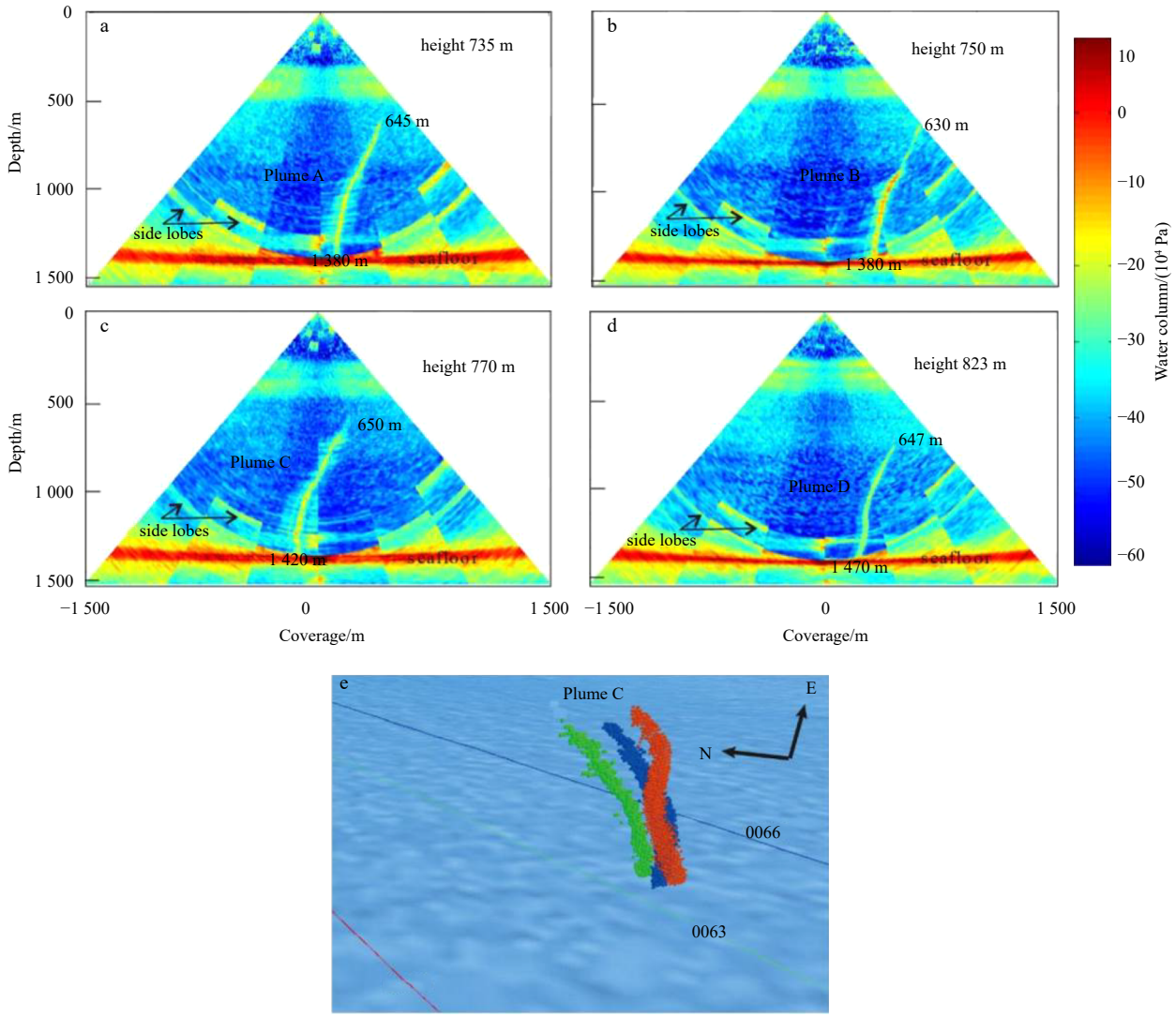

Fig. 2. The water column images of gas bubble plumes (a, b, c and d), and the water column images of Plume C from different multibeam lines (0060, 0063 and 0066) (e). In a, b, c and d, the water depths of the four plumes where they disappear are 645 m, 630 m, 650 m, and 647 m; the corresponding seafloor water depths are 1 380 m, 1 380 m, 1 420 m, and 1 470 m; thus the vertical lengths of the plumes, namely "height", are 735 m, 750 m, 770 m, and 823 m, respectively. In e, the interval between successive lines is 3 h. Plume C is inclined to the northeast at all the three survey lines. The shape of Plume C seems to change over time, but its upper limit seems to be almost invariant (640 m ± 10 m).

m in height, respectively (Figs 2a–d). All of them disappear at water depths of ~640 m. The diameters of these plumes are 30–50 m. The Plume C, closest to Site ROV2, has been sampled by three different multibeam lines and shown in a 3D view (Fig. 2e). The shape of Plume C varies within three hours, while the height is almost constant.

The bathymetric data from the study area show a gentle slope (ca. 0.26°) from southwest to northeast. The water depth ranges from 1 350 m to 1 450 m. Deepwater channels are observed in the upper slopes of the basin (Fig. 3a). However, the backscatter pattern indicates the northeast direction of bottom current flow (Fig. 3b), corresponding to the direction indicated by Plume C.

4.2 *Subsurface structures of active Haima cold seeps*

4.2.1 *Bubble Plume B and subsurface structures*

Seismic profile traversing Plume B show an irregular basement topography consisting of three basement uplifts, labeled as Uplifts 1 to 3, from SE to NW, respectively (Fig. 4a). For the convenience of description, the subsurface structure beneath Plume B can be divided into three parts, i.e., Part 1 (from CDP 3 000 to the southeast), Part 2 (from CDP 3 000 to 6 500), and Part 3 (from CDP 6 500 to the northwest). In Part 2, seismic reflections above Uplifts 1 and 2 are characterized by dimmed amplitude and discontinuity, indicating two distinct large gas chimneys (GC1 and GC2) (Fig. 4a). Reflection events are dimmed in the interior of the gas chimneys, with some discontinuous subparallel reflections visible. Instead, the sediments at the same depth above Uplift 3 are stratified but highly faulted. Moreover, at about 2.6 s two-way traveltime (TWT), a bright spot is found on the top of the highly-faulted zone above the crest of Uplift 3. A minor gas chimney (GC3) with a diameter of ca. 300 m is located directly above this bright spot (Fig. 4a).

GC1 and GC2 are topped by the bottom simulating reflectors (BSRs) with reverse polarity at ~2.1 s TWT, above which a distinct acoustic blanking zone exists (Fig. 4a). Minor fluid expul-

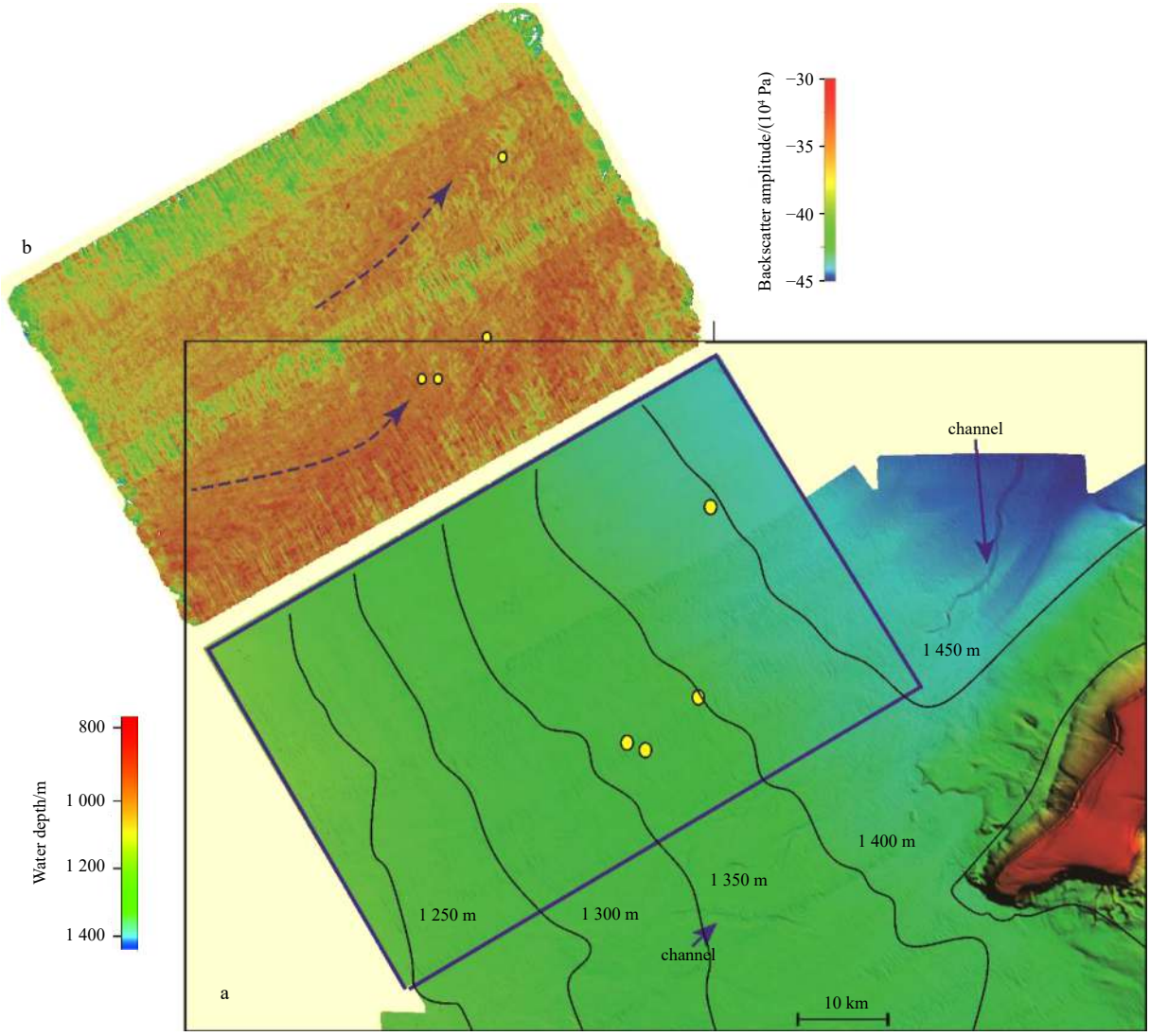

Fig. 3. Bathymetry (a) and backscatter data show seafloor geomorphological and acoustic sedimentary details (b). Note that the Haima cold seeps are located on a gentle slope.

sion anomalies are observed between the seafloor and the acoustic blanking zone (Fig. 4b). A small-scale vertical amplitude anomaly manifested as stacked high amplitude reflection extends from the BSRs through the blanking zone to the seafloor, and connects to Plume B. Moreover, a minor depression occurs at the flat seafloor at the site of Plume B.

4.2.2 *Bubble Plume C and subsurface structures*

A flat, prominent basement uplift reaching over 10 km in length is observed beneath Plume C (Fig. 5a). A giant gas chimney, approximately 11 km in diameter, manifested in the almost absence of internal reflections, develops between the basement uplift and the overlying BSRs. The likely pull-up feature is observed on the inner sides of the gas chimney (Fig. 5b). The BSRs with poor continuity lie at ~2.1 s TWT and are crosscut by substantial fractures. Two acoustic blanking zones exist above the BSRs, separated by a chaotic, stair-step, high amplitude reflection zone. Interestingly, the BSRs shoal sequentially along NE direction, and the sites of pockmarks and Plume C coincide with the lateral change points of the BSRs. Three vertical amplitude anomalies, corresponding to the three seafloor anomalies (PM1, PM2 and Plume C), share comparable features with the vertical amplitude anomalies below Plume B (Fig. 4b), but the difference is that they do not obviously extend to the underlying blanking zone. The vertical continuities of such amplitude anomalies below PM2 and Plume C are more distinct than that below PM1 (Figs 5c and d). In addition, the morphology of PM2 is significantly different from that of PM1. PM1 is typical of a distinct depression on the seafloor, whereas a small mound lies in the center of PM2 (Fig. 5c).

4.2.3 *Bubble Plume D and subsurface structures*

Relative to other sites, the gas chimney beneath Plume D is defined by much smaller size and is located above the slope area of the basement (Fig. 6a). The gas chimney, approximately 1 km in diameter, from CDP 4 000 to CDP 4 500, disturbs the BSRs and terminates below a V-shaped lump of enhanced amplitudes with chaotic and heterogeneous facies (Fig. 6b). The BSRs characterize less disturbance than the BSRs beneath Plume C, with only partial fluctuations and break. Several acoustic blanking zones are interbedded in the strata above the BSRs. Different from the vertical amplitude anomalies observed beneath Plumes B and C

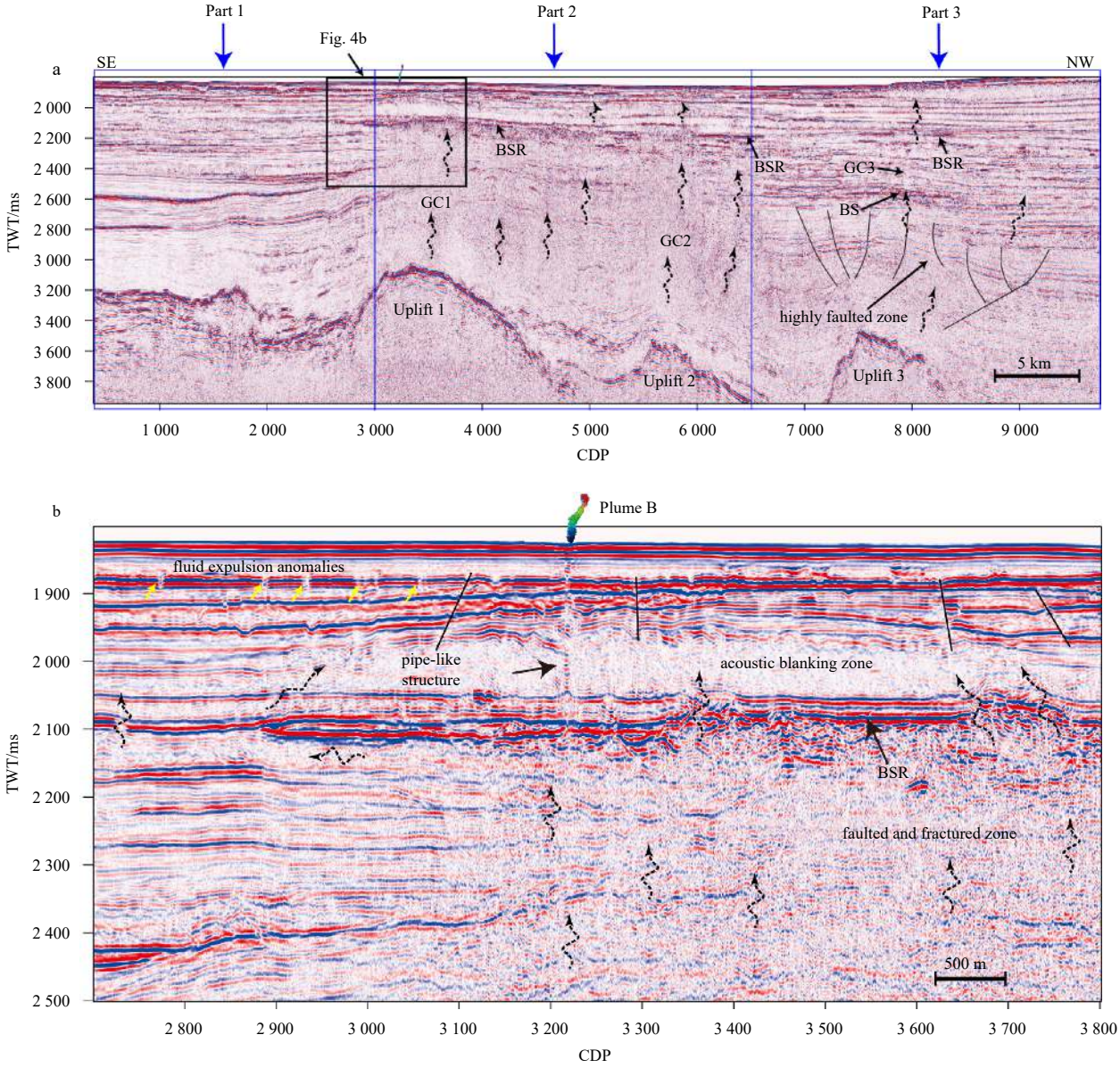

Fig. 4. Seismic expressions of the fluid process associated with Plume B. a. The 2D seismic line 1236 passing through Plume B, showing the uplifted basements and the overlying gas chimneys; and b. the detailed image of the zone denoted by the black box in Fig. 4a, which illustrates the faulted zone and the BSRs on the top of GC1. In a, the location of the seismic line is depicted in Fig. 1b, and the section is divided into three parts for further discussion. In b, an acoustic blanking zone is directly above the BSRs, through which a pipe-like structure rises to the seafloor and connects to Plume B. Wispy fluid expulsion anomalies, perhaps paleo-pockmarks, are indicated by yellow arrows. GC: gas chimney, BS: bright spot, BSR: bottom simulating reflector.

(Figs 4b and 5b), a deflecting amplitude anomaly can be identified just beneath Plume D. There are some enhanced reflections on the flanks of the gas chimney. On the SE side, a dome-shaped anomaly with high amplitude occurs, above which the reflections exhibit the same upward-bending feature. On the NW side, the enhanced reflections are more extensive and exhibit a stronger continuity.

Plume D is the only one within a 3D seismic survey zone and its subsurface structures can be further analyzed using the available 3D seismic dataset. From the time slice of the 3D seismic volume at 2 300 ms TWT (Fig. 7a), the gas chimney in the horizontal plane appears to be an oval shape with low amplitude inside and high amplitude in the surrounding. In almost the same location, a low RMS amplitude zone is depicted from the slice of RMS amplitude attribute along the BSRs, with an extremely high RMS amplitude zone to the NW (Fig. 7b). High RMS amplitude zones are mainly distributed in the NW and SE of the attribute slice. In the NW, the high-value anomalies are in the form of clumps and granules, while the high-value anomalies are principally diffuse in the SE. Note that there is a medium-high RMS amplitude zone in the north of the attribute slice.

5 Discussion

5.1 *Fate of gas bubble plumes*

Methane is a more potent greenhouse gas than carbon dioxide and may contribute to global warming. It is still a debate whether the methane released from the seabed can reach the at-

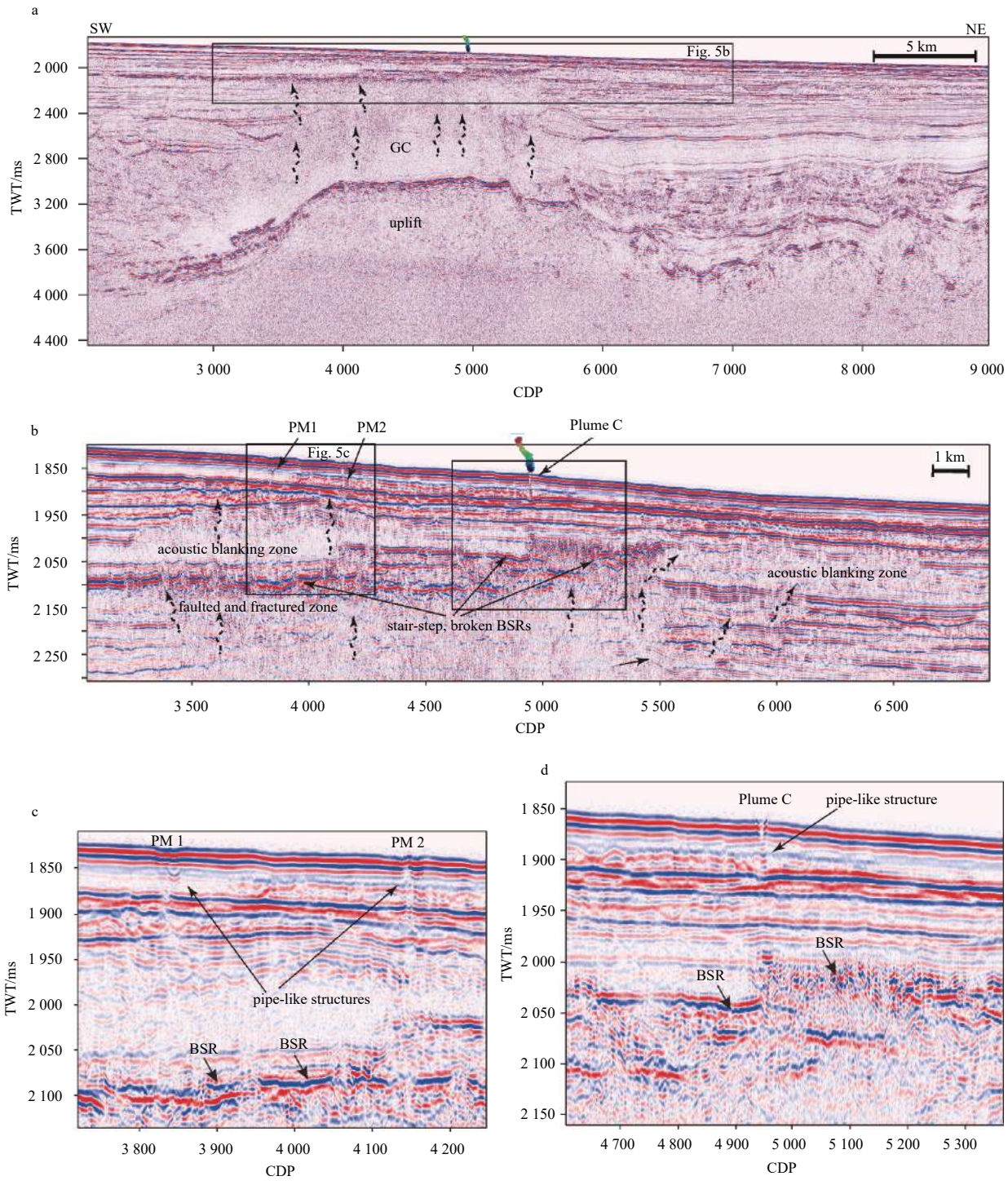

Fig. 5. Seismic expressions of the fluid process associated with Plume C. a. Seismic section of MCS line L440 passing through Plume C, showing a basement uplift with a flat roof, topped by a large-scale gas chimney; and b. detailed image of the zone marked by the black box in Fig. 5a. In addition to Plume C, pockmarks (PM1 and PM2) are observed. The acoustic blanking zones and vertical amplitude anomalies are also shown between the seafloor and the BSRs. c. Zoomed figure showing PM1, PM2 and the corresponding underlying vertical anomalies; and d. zoomed figure showing the detailed structure beneath Plume C. GC: gas chimney, PM: pockmark, BSR: bottom simulating reflector, TWT: two-way traveltime.

mosphere (Archer, 2007; Isaksen et al., 2011; Myhre et al., 2016; Ruppel and Kessler, 2017). To reach the atmosphere, methane should not be oxidized during the ascending process in the water column. Hydrate-skin is a mechanism that is proposed to explain why the formation of hydrates in the exterior of venting underwater gases prevents gas bubbles from being oxidized in the water (Rehder et al., 2002; Sauter et al., 2006; Warzinski et al., 2014; Li and Huang, 2016). Thus, gas bubble plumes may disappear near the upper limit of the stability zone of the gas hydrates.

Gas hydrate stability zone (GHSZ) in the ocean is calculated

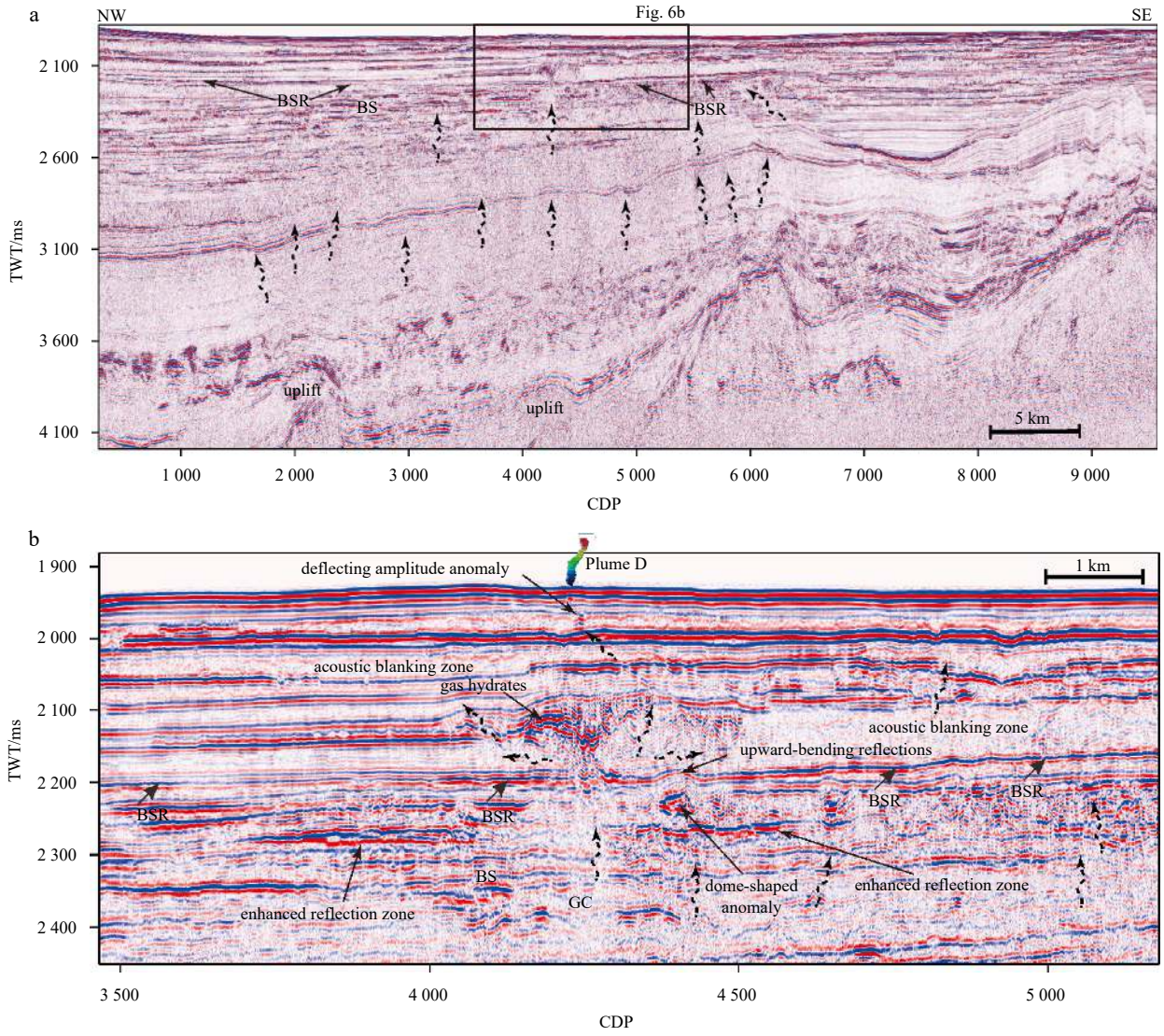

Fig. 6. Seismic expressions of the fluid process associated with Plume D. a. Seismic section of the MCS line 1 218 passing through Plume D, showing a rough, fluctuant basement and a minor gas chimney; and b. detailed image of the zone marked by the black box in Fig. 6a. Enhanced reflection zones occur beneath the BSRs. Acoustic blanking zones emerge in the overlying strata. Atop of the gas chimney, a V-shaped anomaly exists, corresponding to the deflecting amplitude anomaly and Plume D. GC: gas chimney, BS: bright spot, BSR: bottom simulating reflector, TWT: two-way traveltime.

using the CSMHYD program (Sloan, 1998). Shipboard analysis of the head-space gas showed the absolute advantage of methane (Yang et al., 2018). Therefore, pure methane is assumed. Based on the temperature data obtained from the CTD within the study area, GHSZ within the water column is displayed in Fig. 8. All four plumes extend from ~1 400 m below the sea level and disappear at 630–650 m below the sea level, regardless of the water depth. The upper limit of GHSZ calculated from the CTD data is about 620 m. Therefore, gas bubble plumes disappear before they reach the upper limit of the GHSZ in the water. The depths where gas plumes disappear are very close to the upper limit of GHSZ that is calculated from the CTD data (Table 1). The minor discrepancy (about 10–30 m) between them can be caused by many factors, such as the gas composition, inaccurate CTD data, and the various hydrate decomposition rate. Therefore, our observations support the "hydrate skin" hypothesis. Heeschen et al. (2003) have a similar conclusion based on the coincidence of the depths at which gas flares disappear and the predicted depth of the GHSZ boundary.

Water column data acquired at three hours interval show that the shape of the plumes has great variations at the scale of ~3 h, which may indicate a short-scale temporal variation in the methane flux. If methane flux of the Haima cold seeps is to be estimated in the future, the short-scale temporal flux variation must be considered and continuous observations for a long time are necessary, otherwise serious deviations may occur just on the basis of the interpolation and extrapolation of limited observations.

5.2 *Mechanisms of gas migration, gas hydrate accumulations, and seepage*

5.2.1 *Gas chimneys below the BSRs*

Gas chimneys, topped by BSRs with high amplitude, are observed beneath all plumes, which suggests that gas chimneys are essential pathways for gas migration from deep gas reservoirs to shallow sediments at the Haima cold seeps. Gas chimneys be-

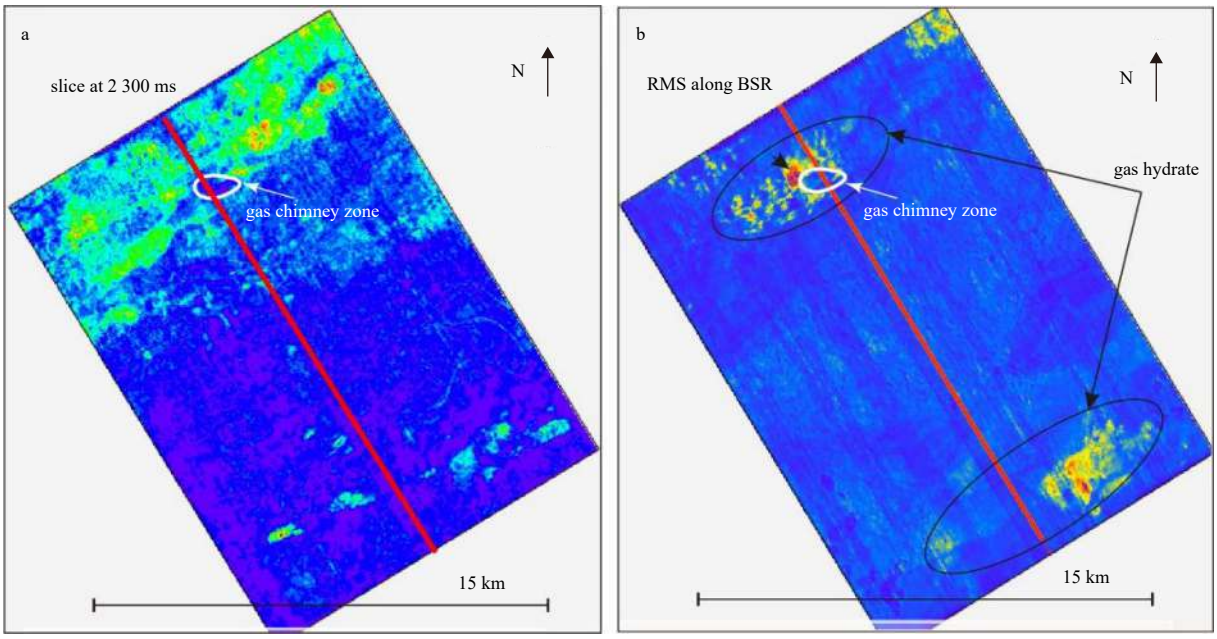

Fig. 7. Seismic attributes associated with the cold seep. a. Time slice of the 3D seismic volume at 2 300 ms two-way traveltime; and b. RMS amplitude attribute derived from the 3D seismic volume. The red lines indicate the locations of part of the Line 1218 which passes through Plume D. The area where the gas chimney developed exhibits low-value features in both slices. In addition, several medium-high and high-value zones are observed in the north, northwest, and southeast of RMS amplitude attribute slice. BSR: bottom simulating reflector.

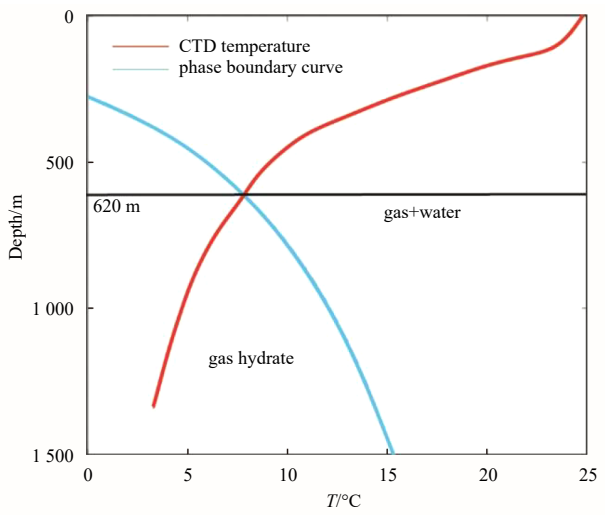

Fig. 8. Hydrate stability phase diagram and the CTD temperature results. The intersection of the hydrate phase boundary curve (blue line) with the temperature curve (red line) defines the upper limit of the GHSZ in the water.

neath Plumes B and C, with several kilometers in diameter and dimmed internal structure, develop above the basement uplift (Figs 4 and 5), where faults and fractures form easily in the vicinity due to disequilibrium compaction and probable denudation (Liang et al., 2019). Numerous subvertical faults within the gas chimney beneath Plume C have been imaged (Wei et al., 2020). Although the faults and fractures within GC1 and GC2 are hard to discern due to the presence of gas, a highly faulted zone is depicted above the uplift in Part 3. In addition, in the QDNB, an uplift area is often deemed as a favorable zone of hydrocarbon migration from the sag center to structural high through lateral permeable layers and the slope of the uplift (Zhu et al., 2009). Thus, gas migrates from the top of uplift to the shallow depths through the fracture networks, forming these gas chimneys, as documented by the bright spot and the minor gas chimney (GC3) directly above the highly faulted zone (Fig. 4a). In contrast, the gas chimney beneath Plume D is defined by a much smaller size and is located above the slope area of the basement (Fig. 6). We speculate that it may derive from *in situ* generation and accumulation of biogenic gas or the transition of gas from lateral advection along the underlying inclined stratigraphic layers to vertical advection through the localized highly fractured zone.

5.2.2 *Gas migration into the GHSZ and occurrence of gas hydrate*

As indicated by the BSRs on the top of all gas chimneys, the ascending gas through gas chimneys has entered into the GHSZ and induced the formation of gas hydrate. The acoustic blanking zone overlying the BSRs is often indicative of the gas hydrate layer (Figs 4–6), as the results of the cementation of the stratal interfaces by the gas hydrate molecules (Hyndman and Spence, 1992; Diaconescu et al., 2001), or merely caused by lithologic homogeneity of sediments (Holbrook et al., 1996). Continuous gas influx into the GHSZ gives rise to the enrichment of gas hydrates and the formation of authigenic carbonates in the shallow subsurface, then the pore space will be clogged and the permeability of the fractures via which gas moves upward will decrease (Loher et al., 2018). The occurrence of massive gas hydrate accumulations may be inferred from the seismic reflection complexes with strong amplitudes above the BSRs (Figs 5b and 6b), because enhanced reflection amplitude in the GHSZ is often used as an indicator of gas hydrate (Yoo et al., 2013). Under the sealing effect exerted by the gas hydrate layer, vertical migration of gas is likely restricted and gas accumulates below the BSRs, thus favoring the

Table 1. Differences of the seismic expressions and plumes at the four seep sites

Site	Seismic anomalies about fluid migration	Conduit (pipe-like structure)	Water depth of termination of plume/mbsl	Diameter of the root of plumes/m
A	/	/	645	26
B	gas chimney (>10 km wide), bright spot, paleo-pockmarks (?)	strictly columnar, high amplitude	630	28
C	gas chimney (>10 km wide), pockmarks	diffuse, dimmed amplitude	650	50
D	gas chimney (~1 km wide), enhanced reflections, bright spot, dome-shaped anomaly	deflecting, moderate amplitude	647	33

Note: "/" indicates that the corresponding feature is not found, and mbsl means m below the sea level.

build-up of over-pressure and the lateral advection of gas within permeable rocks. Pore fluid analysis between ROV1 site and the nearby sites has exemplified such diversion of migration paths at the Haima cold seeps (Hu et al., 2019). Since high amplitude reflections below the BSR appear to be ascribed to the presence of free gas within sediments (Holbrook et al., 1996; Bünz et al., 2003; Yoo et al., 2013), as displayed in Fig. 6b, the enhanced reflections on the sides of the gas chimney and the dome-shaped anomaly below the BSRs may represent gas charging local patches of permeable beds and localized gas accumulation, respectively. Noticeably, as indicated by the distortion of the reflectors immediately above, the overlying sediments have deformed invoked by the dome-shaped anomaly, that may arise from high pressure within the gas accumulation, or may partially be associated with the growth of gas hydrate lenses (Hovland and Svensen, 2006; Paull et al., 2008).

Gas hydrate occurrence below the BSR has been proven by the samples recovered offshore NW Borneo (Paganoni et al., 2016) and the logging-while-drilling data in the Shenhu area of the PRMB during the GMGS3 to GMGS6 expedition (Zhang et al., 2017; Qian et al., 2018; Jin et al., 2020; Qin et al., 2020). Moreover, conclusive evidence for gas hydrate below the BSR has been obtained during the GMGS5 expedition in the QDNB where the gas hydrate system is also closely connected with an underlying gas chimney, and both thermogenic gas and biogenic gas are responsible for the formation of gas hydrate below the BSR (Ye et al., 2019; Liang et al., 2019). Piston and gravity cores collected from the Haima cold seeps have demonstrated the contributions of thermogenic gas and biogenic gas (Fang et al., 2019; Feng et al., 2019). The base of gas hydrate stability zone (BGHSZ) may extend much deeper than suggested by the BSR in the thermogenic gas-dominated setting (Paganoni et al., 2016). Even if we have no direct seismic evidence, given that the Haima cold seeps have the similar geological features (e.g., gas hydrate system sourced by a gas chimney developing above the uplift) to those of the GMGS5 drilling area (Wei et al., 2019; Ye et al., 2019; Liang et al., 2019), as well as the petroleum geological conditions in the QDNB (Ma et al., 2008; Li et al., 2012; He et al., 2013, 2015; Huang et al., 2014, 2016; Zhang et al., 2016), we propose that it is plausible for gas hydrate occurrence below the BSR, which is also revealed by the pull-up feature on the inner sides of the gas chimneys (Fig. 5b). Nevertheless, further investigations, such as long cores penetrating through these gas chimneys and precise velocity analysis, are necessary to verify the occurrence and distribution of gas hydrate below the BSR in the study area.

Once the pore pressure exceeds a critical value, local hydro-fracturing of the overburden including the BGHSZ is invoked. Then free gas trapped by the gas hydrate layer migrates upward into the overlying gas hydrate-bearing sediments through hydro-fractures and tectonic fractures (Petersen et al., 2010). The BSRs, especially beneath Plume C, are featured by poor continuity, which may imply that extensive hydro-fracturing has occurred. Additionally, the seismic profiles show a pattern of the BSRs that the degree of discontinuity seems to be positively correlated with the size of gas chimney, highlighting the effect of gas supply on the gas hydrate system. Gas emission induces pore pressure decrease in the shallow sediments so that the fractures are clogged by gas hydrates again and cannot conduit fluids, which in turn leads to re-build-up of pressure and consequent gas emission (Wei et al., 2020).

5.2.3 *Gas seeping into the water column*

In addition to forming hydrates, sufficient and sustained gas entering into the GHSZ migrates upwards to the seafloor and escapes, further inducing the formation of gas plumes and pockmarks (Figs 4–6). Faults, fractures, sediment mobilizations, pipes, and seismic chimneys are common conduits for seabed fluid escape (Cartwright et al., 2007; Haacke et al., 2009; Løseth et al., 2009; Andresen, 2012; Karstens and Berndt, 2015). Wang et al. (2018b) and Wei et al. (2020) suggest that fractures and minor faults are the primary pathways within the shallow sediments for gas seeping into the water column at the Haima cold seeps. However, based on our seismic data, vertical amplitude anomalies just below all plumes and pockmarks, characterized by stacked high amplitude reflections or vertical discontinuity zone diffuse with depth, are clearly imaged and interpreted as fluid conduits transporting gas to the seafloor (Figs 4–6). Comparable with the observations from seismic pipe structures (Løseth et al., 2011; Gay et al., 2012; Maestrelli et al., 2017; Hustoft et al., 2007), we prefer to term these vertical amplitude anomalies herein as pipe-like structures.

The characteristic of these pipe-like structures appears to, at least to some extent, reflect the dynamic process of gas seepage. The strictly columnar pipe-like structure below Plume B may indicate a more focused, persistent seepage (Fig. 4b). Its high amplitude may be either ascribed to free gas inside or the accumulation of gas hydrate along this fluid conduit.

Conversely, the pipe-like structures below the pockmarks and Plume C are relatively indistinct and diffuse (Figs 5c and d). Pockmarks are often seen as remnants of gas emissions (Judd and Hovland, 2007), while the site of Plume C where mussels covered large area is suggested as a young active seep (Wei et al., 2020). Focused gas seepage, i.e. gas plumes, will terminate as the pore fluid pressure drops, and associated feeder pipe will be plugged, collapse, or alter in later geological processes (Løseth et al., 2011), which may account for the indistinct pipe-like structures below PM1 and PM2. Moreover, comparison of their positions with the underlying BSRs reveals a spatial coincidence between seepage sites and the points where the BSRs shoal sequentially along NE direction (Fig. 5b). Local shoaling of the BSR, opposite to the seabed topography, tend to be associated with enhanced gas flux (Schwalenberg et al., 2010; Wei et al., 2019). These observations, together with the BSRs with poor continuity, may imply that the focused gas expulsion is possibly determined

by the episodically active, progressively enhanced, plumbing system including the pipe-like structure, the fracture network, as well as the subjacent gas chimney, which may be controlled by the build-up and dissipation of pressure as mentioned above.

However, we cannot determine the feeder pipe of Plume D although there is a deflecting amplitude anomaly just below. It is speculated that the formation of Plume D may be linked to the underlying gas hydrate accumulation due to the clear spatial superimposed relationship of Plume D with the deflecting amplitude anomaly and the gas hydrate accumulation (Fig. 6b).

5.3 *Links between gas chimneys and gas hydrate accumulations*

All seismic profiles reveal that the gas chimney acts as the crucial pathway for gas migrating into shallow stratum, leading to the formation and accumulation of gas hydrate. However, the control of gas chimney on gas hydrate accumulation is still equivocal. In the light of the detailed 3D seismic data, the links between gas chimneys and gas hydrate accumulations are evaluated by comparing their spatial distributions.

The cross-section of the gas chimney appears to be an oval shape with low amplitude (Fig. 7a), consistent with the gas chimney reported in ZRMB (Sun et al., 2012). The seismic profile shows that the top of this gas chimney has reached the BSRs (Fig. 6b). Gas hydrate accumulation is highlighted by high RMS amplitude (Plaza-Faverola et al., 2010). Thus, two zones of gas hydrate accumulation are identified, one around the gas chimney while the other in the southeast (Fig. 7b). Massive gas hydrates are observed concentrated on the periphery of the gas chimney and may be characterized by high saturation, as indicated by the maximum RMS amplitudes. In areas away from the chimney, gas hydrates are more dispersed and less saturated. The results suggest that gas chimney provides favorable conditions for the accumulation of gas hydrate with high saturation. The periphery of a gas chimney may be an ideal target for future gas hydrate exploration in the QDNB. Similar gas chimneys in relation to high hydrate saturation are confirmed in various settings, including the northern Cascadia Margin (Riedel et al., 2006), the Ulleung Basin (Chun et al., 2011), the Shenhu area in the ZRMB (Zhang et al., 2017) and the GMGS5 drilling area in the QDNB (Wei et al., 2019; Ye et al., 2019; Liang et al., 2019).

5.4 *Model of gas hydrate system and seepage at the Haima cold seeps*

According to the interpretations of seismic data, we hypothesize the following evolutionary model for the development of the gas hydrate system and the gas seepage in the study area (Fig. 9).

Thermogenic gas migrates from the source layers in the sags adjacent to both sides of the basement uplift, through lateral permeable stratigraphic layers and the slope of the uplift, to the top of the uplift. Thermogenic gas moves upwards by charging the faults and fractures in the overlying strata and mixes with the biogenic gas generated from the shallow formations, responsible for the formation of the major gas chimney (Fig. 9a). In some cases, minor gas chimney develops when gas charges into localized zones with strong permeability.

The gas migrates into the GHSZ through the gas chimneys,

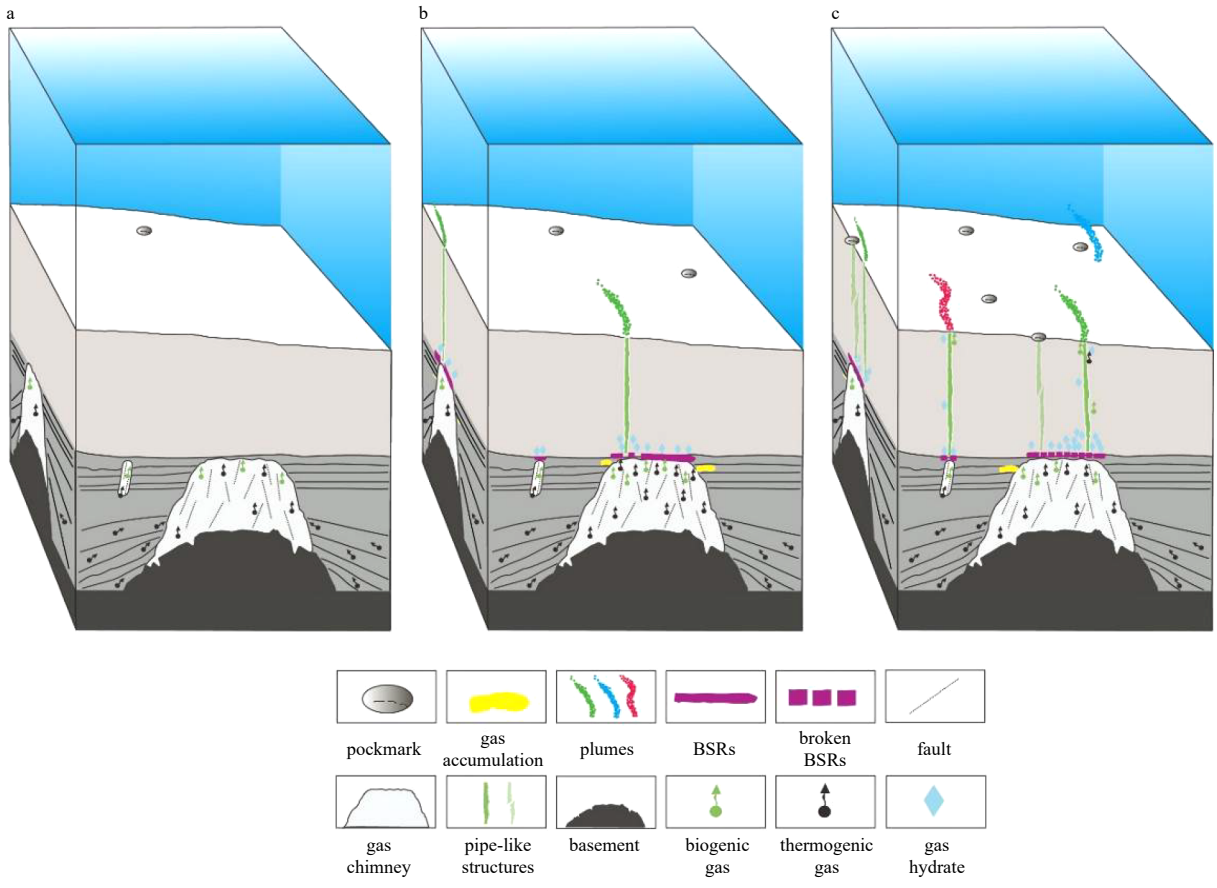

Fig. 9. The schematic diagram of the model of gas migration, gas hydrate accumulation, and the related seepage at the Haima cold seeps. BSRs: bottom simulating reflectors.

then gas hydrates begin to form and fill the sediment pore space. With the gradual enrichment of gas hydrates, gas hydrates tend to accumulate on the periphery of the gas chimney and hinder the further upward-moving of the free gas. Continuous gas influx induces the accumulation of free gas below the gas hydrate layer, which is conducive to the build-up of overpressure and the lateral advection of gas within permeable beds (Fig. 9b). Hydro-fracturing is invoked when the pore pressure exceeds a critical value. Subsequently, substantial gas-rich fluids migrate into the overlying gas hydrate-bearing sediments via the generated hydro-fractures and/or the reactivation of pre-existing fractures. A fraction of gas eventually escapes into the water column driven by pressure through pipe-like structures.

However, the pore pressure drops with the gas release so that the permeability of the original fractures decreases and the gas entering the shallow sediments is restricted. On one hand, due to the lack of enough gas influx and pore pressure, the plugging, collapse, or alteration of the pipe-like structures are induced. Then the gas plumes terminate. On the other hand, the pressure will be re-built-up as free gas accumulates, facilitating consequent gas emission (Fig. 9c). The build-up and dissipation of pressure may account for the dynamic gas seepage at the Haima cold seeps.

6 Conclusions

The shapes of plumes at the Haima cold seeps are variable and influenced by the northeastward bottom current, but the water depth where these gas plumes disappear is very close to the theoretical calculation of the upper limit of the gas hydrate stability zone, supporting the “hydrate skin” hypothesis.

Plume B and C develop above the basement uplift while Plume D is located above the slope area of the basement. The gas chimney acts as the dominating pathway for both thermogenic gas and biogenic gas migrating upward into the GHSZ, leading to the accumulation of gas hydrate in the shallow sediments, particularly on the periphery of the gas chimney. It is speculated that the gas hydrate clogs the pore space, and subsequent overpressure-driven hydrofracturing derived from the underlying free gas accumulation may account for the broken BSRs. The pipe-like structure is considered as the primary conduit conveying gas from the BSRs to the seafloor, feeding the gas plume in the study area. The differences between these pipe-like structures appear to be related to the dynamic process of gas seepage, which may be controlled by the build-up and dissipation of pore pressure. The strictly columnar pipe-like structure may indicate a more focused, persistent seepage while the indistinct pipe-like structure may indicate a terminative or young seepage.

Acknowledgements

We thank the Guangzhou Marine Geological Survey for their permission to release the seismic data. Lijie Wang is thanked for his constructive comments to the manuscript.

References

Andresen K J. 2012. Fluid flow features in hydrocarbon plumbing systems: What do they tell us about the basin evolution?. Marine Geology, 332–334: 89–108, doi: 10.1016/j.margeo.2012.07.006

Archer D. 2007. Methane hydrate stability and anthropogenic climate change. Biogeosciences, 4(4): 521–544, doi: 10.5194/bg-4-521-2007

Bai Yang, Song Haibin, Guan Yongxian, et al. 2014. Structural characteristics and genesis of pockmarks in the northwest of the South China Sea derived from reflective seismic and multibeam data. Chinese Journal of Geophysics (in Chinese), 57(7): 2208–2222

Bangs N L B, Hornbach M J, Berndt C. 2011. The mechanics of intermittent methane venting at South Hydrate Ridge inferred from 4D seismic surveying. Earth and Planetary Science Letters, 310(1–2): 105–112, doi: 10.1016/j.epsl.2011.06.022

Barnard A, Sager W W, Snow J E, et al. 2015. Subsea gas emissions from the Barbados accretionary complex. Marine and Petroleum Geology, 64: 31–42, doi: 10.1016/j.marpetgeo.2015.02.008

Brothers D S, Ruppel C, Kluesner J W, et al. 2014. Seabed fluid expulsion along the upper slope and outer shelf of the U.S. Atlantic continental margin. Geophysical Research Letters, 41(1): 96–101, doi: 10.1002/2013GL058048

Brothers L L, Van Dover C L, German C R, et al. 2013. Evidence for extensive methane venting on the southeastern U.S. Atlantic margin. Geology, 41(7): 807–810, doi: 10.1130/G34217.1

Bünz S, Mienert J, Berndt C. 2003. Geological controls on the Storegga gas-hydrate system of the Mid-Norwegian Continental Margin. Earth and Planetary Science Letters, 209(3–4): 291–307, doi: 10.1016/S0012-821X(03)00097-9

Cartwright J, Huuse M, Aplin A. 2007. Seal bypass systems. AAPG Bulletin, 91(8): 1141–1166, doi: 10.1306/04090705181

Chen Jiangxin, Guan Yongxian, Song Haibin, et al. 2015a. Distribution characteristics and geological implications of pockmarks and mud volcanoes in the northern and western continental margins of the South China Sea. Chinese Journal of Geophysics (in Chinese), 58(3): 919–938

Chen S C, Hsu S, Wang Y, et al. 2014. Distribution and characters of the mud diapirs and mud volcanoes off southwest Taiwan. Journal of Asian Earth Sciences, 92: 201–214, doi: 10.1016/j.jseaes.2013.10.009

Chen Duofu, Huang Yongyang, Yuan Xunlai, et al. 2005. Seep carbonates and preserved methane oxidizing archaea and sulfate reducing bacteria fossils suggest recent gas venting on the seafloor in the Northeastern South China Sea. Marine and Petroleum Geology, 22(5): 613–621, doi: 10.1016/j.marpetgeo.2005.05.002

Chen Jiangxin, Song Haibin, Guan Yongxian, et al. 2015b. Morphologies, classification and genesis of pockmarks, mud volcanoes and associated fluid escape features in the northern Zhongjiannan Basin, South China Sea. Deep Sea Research Part II: Topical Studies in Oceanography, 122: 106–117, doi: 10.1016/j.dsr2.2015.11.007

Chen Jiangxin, Song Haibin, Guan Yongxian, et al. 2018. Geological and oceanographic controls on seabed fluid escape structures in the northern Zhongjiannan Basin, South China Sea. Journal of Asian Earth Sciences, 168: 38–47, doi: 10.1016/j.jseaes.2018.04.027

Chun J H, Ryu B J, Son B K, et al. 2011. Sediment mounds and other sedimentary features related to hydrate occurrences in a columnar seismic blanking zone of the Ulleung Basin, East Sea, Korea. Marine and Petroleum Geology, 28(10): 1787–1800, doi: 10.1016/j.marpetgeo.2011.06.006

Crutchley G J, Klaeschen D, Planert L, et al. 2014. The impact of fluid advection on gas hydrate stability: investigations at sites of methane seepage offshore Costa Rica. Earth and Planetary Science Letters, 401: 95–109, doi: 10.1016/j.epsl.2014.05.045

Diaconescu C C, Kieckhefer R M, Knapp J H. 2001. Geophysical evidence for gas hydrates in the deep water of the South Caspian Basin, Azerbaijan. Marine and Petroleum Geology, 18(2): 209–221, doi: 10.1016/S0264-8172(00)00061-1

Etiope G. 2012. Methane uncovered. Nature Geoscience, 5(6): 373–374, doi: 10.1038/ngeo1483

Fang Yunxin, Wei Jiangong, Lu Hailong, et al. 2019. Chemical and structural characteristics of gas hydrates from the Haima cold seeps in the Qiongdongnan Basin of the South China Sea. Journal of Asian Earth Sciences, 182: 103924, doi: 10.1016/j.jseaes.2019.103924

Feng Dong, Qiu Jianwen, Hu Yu, et al. 2018. Cold seep systems in the South China Sea: An overview. Journal of Asian Earth Sciences, 168: 3–16, doi: 10.1016/j.jseaes.2018.09.021

Feng Junxi, Yang Shengxiong, Wang Hongbin, et al. 2019. Methane source and turnover in the shallow sediments to the west of Haima cold seeps on the northwestern slope of the south China

Sea. Geofluids, 2019: 1010824
Foucher J P, Westbrook G K, Boetius A, et al. 2009. Structure and drivers of cold seep ecosystems. Oceanography, 22(1): 92–109, doi: 10.5670/oceanog.2009.11
Gay A, Mourgues R, Berndt C, et al. 2012. Anatomy of a fluid pipe in the Norway Basin: Initiation, propagation and 3D shape. Marine Geology, 332-334: 75–88, doi: 10.1016/j.margeo.2012.08.010
Greinert J, Artemov Y, Egorov V, et al. 2006. 1300-m-high rising bubbles from mud volcanoes at 2080 m in the Black Sea: Hydroacoustic characteristics and temporal variability. Earth and Planetary Science Letters, 244(1–2): 1–15, doi: 10.1016/j.epsl.2006.02.011
Guan Hongxiang, Birgel D, Peckmann J, et al. 2018. Lipid biomarker patterns of authigenic carbonates reveal fluid composition and seepage intensity at Haima cold seeps, South China Sea. Journal of Asian Earth Sciences, 168: 163–172, doi: 10.1016/j.jseaes.2018.04.035
Haacke R R, Hyndman R D, Park K P, et al. 2009. Migration and venting of deep gases into the ocean through hydrate-choked chimneys offshore Korea. Geology, 37(6): 531–534, doi: 10.1130/G25681A.1
Han Xiqiu, Suess E, Huang Yongyang, et al. 2008. Jiulong methane reef: Microbial mediation of seep carbonates in the South China Sea. Marine Geology, 249(3–4): 243–256, doi: 10.1016/j.margeo.2007.11.012
Han Xiqiu, Suess E, Liebetrau V, et al. 2014. Past methane release events and environmental conditions at the upper continental slope of the South China Sea: constraints by seep carbonates. International Journal of Earth Sciences, 103(7): 1873–1887, doi: 10.1007/s00531-014-1018-5
He Jiaxiong, Su Pibo, Lu Zhenquan, et al. 2015. Prediction of gas sources of natural gas hydrate in the Qiongdongnan Basin, northern South China Sea, and its migration, accumulation and reservoir formation pattern. Natural Gas Industry (in Chinese), 35(8): 19–29
He Jiaxiong, Yan Wen, Zhu Youhai, et al. 2013. Bio-genetic and sub-biogenetic gas resource potential and genetic types of natural gas hydrates in the northern marginal basins of South China Sea. Natural Gas Industry (in Chinese), 33(6): 121–134
Heeschen K U, Tréhu A M, Collier R W, et al. 2003. Distribution and height of methane bubble plumes on the Cascadia Margin characterized by acoustic imaging. Geophysical Research Letters, 30(12): 1643
Holbrook W S, Hoskins H, Wood W T, et al. 1996. Methane hydrate and free gas on the Blake ridge from vertical seismic profiling. Science, 273(5283): 1840–1843, doi: 10.1126/science.273.5283.1840
Hovland M, Svensen H. 2006. Submarine pingoes: Indicators of shallow gas hydrates in a pockmark at Nyegga, Norwegian Sea. Marine Geology, 228(1–4): 15–23, doi: 10.1016/j.margeo.2005.12.005
Hu Yu, Luo Min, Liang Qianyong, et al. 2019. Pore fluid compositions and inferred fluid flow patterns at the Haima cold seeps of the South China Sea. Marine and Petroleum Geology, 103: 29–40, doi: 10.1016/j.marpetgeo.2019.01.007
Hu Bo, Wang Liangshu, Yan Wenbo, et al. 2013. The tectonic evolution of the Qiongdongnan Basin in the northern margin of the South China Sea. Journal of Asian Earth Sciences, 77: 163–182, doi: 10.1016/j.jseaes.2013.08.022
Huang Baojia, Tian Hui, Li Xushen, et al. 2016. Geochemistry, origin and accumulation of natural gases in the deepwater area of the Qiongdongnan Basin, South China Sea. Marine and Petroleum Geology, 72: 254–267, doi: 10.1016/j.marpetgeo.2016.02.007
Huang Baojia, Wang Zhenfeng, Liang Gang. 2014. Natural gas source and migration-accumulation pattern in the central canyon, the deep water area, Qiongdongnan Basin. China Offshore Oil and Gas (in Chinese), 26(5): 8–14
Huang Baojia, Xiao Xianming, Li Xushen, et al. 2009. Spatial distribution and geochemistry of the nearshore gas seepages and their implications to natural gas migration in the Yinggehai Basin, offshore South China Sea. Marine and Petroleum Geology, 26(6): 928–935, doi: 10.1016/j.marpetgeo.2008.04.009
Hustoft S, Mienert J, Bünz S, et al. 2007. High-resolution 3D-seismic data indicate focussed fluid migration pathways above polygonal fault systems of the Mid-Norwegian Margin. Marine Geology, 245(1–4): 89–106, doi: 10.1016/j.margeo.2007.07.004
Hyndman R D, Spence G D. 1992. A seismic study of methane hydrate marine bottom simulating reflectors. Journal of Geophysical Research: Solid Earth, 97(B5): 6683–6698, doi: 10.1029/92JB00234
Isaksen I S A, Gauss M, Myhre G, et al. 2011. Strong atmospheric chemistry feedback to climate warming from Arctic methane emissions. Global Biogeochemical Cycles, 25(2): GB2002
Jin Jiapeng, Wang Xiujuan, Guo Yiquan, et al. 2020. Geological controls on the occurrence of recently formed highly concentrated gas hydrate accumulations in the Shenhu area, South China Sea. Marine and Petroleum Geology, 116: 104294, doi: 10.1016/j.marpetgeo.2020.104294
Judd A G. 2003. The global importance and context of methane escape from the seabed. Geo-Marine Letters, 23(3–4): 147–154, doi: 10.1007/s00367-003-0136-z
Judd A, Hovland M. 2007. Seabed Fluid Flow: the Impact on Geology, Biology and the Marine Environment. Cambridge: Cambridge University Press
Karstens J, Berndt C. 2015. Seismic chimneys in the Southern Viking Graben-Implications for palaeo fluid migration and overpressure evolution. Earth and Planetary Science Letters, 412: 88–100, doi: 10.1016/j.epsl.2014.12.017
Klaucke I, Weinrebe W, Petersen C J, et al. 2010. Temporal variability of gas seeps offshore New Zealand: multi-frequency geoacoustic imaging of the Wairarapa area, Hikurangi margin. Marine Geology, 272(1-4): 49–58, doi: 10.1016/j.margeo.2009.02.009
Li Changjun, Huang Ting. 2016. Simulation of gas bubbles with gas hydrates rising in deep water. Ocean Engineering, 112: 16–24, doi: 10.1016/j.oceaneng.2015.12.002
Li Wenhao, Zhang Zhihuang, Li Youchuan, et al. 2012. New perspective of Miocene marine hydrocarbon source rocks in deep-water area in Qiongdongnan Basin of northern South China Sea. Acta Oceanologica Sinica, 31(5): 107–114, doi: 10.1007/s13131-012-0241-9
Liang Qianyong, Hu Y, Feng Dong, et al. 2017. Authigenic carbonates from newly discovered active cold seeps on the northwestern slope of the South China Sea: Constraints on fluid sources, formation environments, and seepage dynamics. Deep Sea Research Part I: Oceanographic Research Papers, 124: 31–41, doi: 10.1016/j.dsr.2017.04.015
Liang Jinqiang, Zhang Wei, Lu Jing'an, et al. 2019. Geological occurrence and accumulation mechanism of natural gas hydrates in the eastern Qiongdongnan Basin of the South China Sea: Insights from site GMGS5-W9-2018. Marine Geology, 418: 106042, doi: 10.1016/j.margeo.2019.106042
Liu Bin, Liu Shengxuan. 2017. Gas bubble plumes observed at north slope of South China Sea from multi-beam water column data. Haiyang Xuebao (in Chinese), 39(9): 83–89
Loher M, Marcon Y, Pape T, et al. 2018. Seafloor sealing, doming, and collapse associated with gas seeps and authigenic carbonate structures at Venere mud volcano, Central Mediterranean. Deep Sea Research Part I: Oceanographic Research Papers, 137: 76–96, doi: 10.1016/j.dsr.2018.04.006
Løseth H, Gading M, Wensaas L. 2009. Hydrocarbon leakage interpreted on seismic data. Marine and Petroleum Geology, 26(7): 1304–1319, doi: 10.1016/j.marpetgeo.2008.09.008
Løseth H, Wensaas L, Arntsen B, et al. 2011. 1000 m long gas blow-out pipes. Marine and Petroleum Geology, 28(5): 1047–1060, doi: 10.1016/j.marpetgeo.2010.10.001
Lüdmann T, Wong H K. 1999. Neotectonic regime on the passive continental margin of the northern south China Sea. Tectonophysics, 311(1–4): 113–138, doi: 10.1016/S0040-1951(99)00155-9
Ma Wenhong, He Jiaxiong, Yao Yongjian, et al. 2008. Characteristics of tertiary sediments and main Source Rocks, Northern South China Sea. Natural Gas Geoscience (in Chinese), 19(1): 41–48
Maestrelli D, Iacopini D, Jihad A A, et al. 2017. Seismic and structural characterization of fluid escape pipes using 3D and partial stack seismic from the Loyal Field (Scotland, UK): a multiphase

and repeated intrusive mechanism. Marine and Petroleum Geology, 88: 489–510, doi: 10.1016/j.marpetgeo.2017.08.016
Myhre C L, Ferré B, Platt S M, et al. 2016. Extensive release of methane from Arctic seabed west of Svalbard during summer 2014 does not influence the atmosphere. Geophysical Research Letters, 43(9): 4624–4631, doi: 10.1002/2016GL068999
Paganoni M, Cartwright J A, Foschi M, et al. 2016. Structure II gas hydrates found below the bottom-simulating reflector. Geophysical Research Letters, 43(11): 5696–5706, doi: 10.1002/2016GL069452
Paull C K, Normark W R, Ussler III B, et al. 2008. Association among active seafloor deformation, mound formation, and gas hydrate growth and accumulation within the seafloor of the Santa Monica Basin, offshore California. Marine Geology, 250(3–4): 258–275, doi: 10.1016/j.margeo.2008.01.011
Petersen C J, Bünz S, Hustoft S, et al. 2010. High-resolution P-Cable 3D seismic imaging of gas chimney structures in gas hydrated sediments of an Arctic sediment drift. Marine and Petroleum Geology, 27(9): 1981–1994, doi: 10.1016/j.marpetgeo.2010.06.006
Plaza-Faverola A, Bünz S, Mienert J. 2010. Fluid distributions inferred from P-wave velocity and reflection seismic amplitude anomalies beneath the Nyegga pockmark field of the mid-Norwegian margin. Marine and Petroleum Geology, 27(1): 46–60, doi: 10.1016/j.marpetgeo.2009.07.007
Prinzhofer A, Deville E. 2013. Origins of hydrocarbon gas seeping out from offshore mud volcanoes in the Nile delta. Tectonophysics, 591: 52–61, doi: 10.1016/j.tecto.2011.06.028
Qian Jin, Wang Xiujuan, Collett T S, et al. 2018. Downhole log evidence for the coexistence of structure II gas hydrate and free gas below the bottom simulating reflector in the South China Sea. Marine and Petroleum Geology, 98: 662–674, doi: 10.1016/j.marpetgeo.2018.09.024
Qin Xuwen, Lu Jingan, Lu Hailong, et al. 2020. Coexistence of natural gas hydrate, free gas and water in the gas hydrate system in the Shenhu Area, South China Sea. China Geology, 3(2): 210–220
Rehder G, Brewer P W, Peltzer E T, et al. 2002. Enhanced lifetime of methane bubble streams within the deep ocean. Geophysical Research Letters, 29(15): 1731
Riedel M, Novosel I, Spence G D, et al. 2006. Geophysical and geochemical signatures associated with gas hydrate-related venting in the northern Cascadia margin. GSA Bulletin, 118(1–2): 23–38, doi: 10.1130/B25720.1
Römer M, Torres M, Kasten S, et al. 2014. First evidence of widespread active methane seepage in the Southern Ocean, off the sub-Antarctic island of South Georgia. Earth and Planetary Science Letters, 403: 166–177, doi: 10.1016/j.epsl.2014.06.036
Ru Ke, Pigott J D. 1986. Episodic rifting and subsidence in the South China Sea. AAPG Bulletin, 70(9): 1136–1155
Ruppel C D, Kessler J D. 2017. The interaction of climate change and methane hydrates. Reviews of Geophysics, 55(1): 126–168, doi: 10.1002/2016RG000534
Sauter E J, Muyakshin S I, Charlou J L, et al. 2006. Methane discharge from a deep-sea submarine mud volcano into the upper water column by gas hydrate-coated methane bubbles. Earth and Planetary Science Letters, 243(3–4): 354–365, doi: 10.1016/j.epsl.2006.01.041
Schwalenberg K, Wood W, Pecher I, et al. 2010. Preliminary interpretation of electromagnetic, heat flow, seismic, and geochemical data for gas hydrate distribution across the Porangahau Ridge, New Zealand. Marine Geology, 272(1–4): 89–98, doi: 10.1016/j.margeo.2009.10.024
Shi Xiaobin, Jiang Haiyan, Yang Jun, et al. 2017. Models of the rapid post-rift Subsidence in the eastern Qiongdongnan Basin, South China Sea: implications for the development of the deep thermal anomaly. Basin Research, 29(3): 340–362, doi: 10.1111/bre.12179
Shi Wanzhong, Xie Yuhong, Wang Zhenfeng, et al. 2013. Characteristics of overpressure distribution and its implication for hydrocarbon exploration in the Qiongdongnan Basin. Journal of Asian Earth Sciences, 66: 150–165, doi: 10.1016/j.jseaes.2012.12.037
Skarke A, Ruppel C, Kodis M, et al. 2014. Widespread methane leakage from the sea floor on the northern US Atlantic Margin. Nature Geoscience, 7(9): 657–661, doi: 10.1038/ngeo2232
Sloan Jr E D. 1998. Clathrate Hydrates of Natural Gases. 2nd ed. New York: Marcel Dekker
Solomon E A, Kastner M, MacDonald I R, et al. 2009. Considerable methane fluxes to the atmosphere from hydrocarbon seeps in the Gulf of Mexico. Nature Geoscience, 2(8): 561–565, doi: 10.1038/ngeo574
Suess E. 2014. Marine cold seeps and their manifestations: geological control, biogeochemical criteria and environmental conditions. International Journal of Earth Sciences, 103(7): 1889–1916, doi: 10.1007/s00531-014-1010-0
Sun Yunbao, Wu Shiguo, Dong Dongdond, et al. 2012. Gas hydrates associated with gas chimneys in fine-grained sediments of the northern South China Sea. Marine Geology, 311–314(1): 32–40, doi: 10.1016/j.margeo.2012.04.003
Tong Hongpeng, Feng Dong, Cheng Hai, et al. 2013. Authigenic carbonates from seeps on the northern continental slope of the South China Sea: New insights into fluid sources and geochronology. Marine and Petroleum Geology, 43: 260–271, doi: 10.1016/j.marpetgeo.2013.01.011
Wang Xudong, Li Niu, Feng Dong, et al. 2018a. Using chemical compositions of sediments to constrain methane seepage dynamics: a case study from Haima cold seeps of the South China Sea. Journal of Asian Earth Sciences, 168: 137–144, doi: 10.1016/j.jseaes.2018.11.011
Wang Lijie, Sun Zhen, Yang Jinhai, et al. 2019. Seismic characteristics and evolution of post-rift igneous complexes and hydrothermal vents in the Lingshui sag (Qiongdongnan Basin), northwestern South China Sea. Marine Geology, 418: 106043, doi: 10.1016/j.margeo.2019.106043
Wang Jiliang, Wu Shiguo, Kong Xiu, et al. 2018b. Subsurface fluid flow at an active cold seep area in the Qiongdongnan Basin, northern South China Sea. Journal of Asian Earth Sciences, 168: 17–26, doi: 10.1016/j.jseaes.2018.06.001
Warzinski R P, Lynn R, Haljasmaa I, et al. 2014. Dynamic morphology of gas hydrate on a methane bubble in water: observations and new insights for hydrate film models. Geophysical Research Letters, 41(19): 6841–6847, doi: 10.1002/2014GL061665
Wei Jiangong, Li Jiwei, Wu Tingting, et al. 2020. Geologically controlled intermittent gas eruption and its impact on bottom water temperature and chemosynthetic communities—A case study in the "HaiMa" cold seeps, South China Sea. Geological Journal, 55(9): 6066–6078, doi: 10.1002/gj.3780
Wei Jiangong, Liang Jinqiang, Lu Jingan, et al. 2019. Characteristics and dynamics of gas hydrate systems in the northwestern South China Sea—Results of the fifth gas hydrate drilling expedition. Marine and Petroleum Geology, 110: 287–298, doi: 10.1016/j.marpetgeo.2019.07.028
Westbrook G K, Thatcher K E, Rohling E J, et al. 2009. Escape of methane gas from the seabed along the West Spitsbergen continental margin. Geophysical Research Letters, 36(15): L15608
Yang Li, Liu Bin, Xu Mengjie, et al. 2018. Characteristics of active cold seepages in Qiongdongnan Sea area of the northern South China Sea. Chinese Journal of Geophysics (in Chinese), 61(7): 2905–2914
Ye Jianliang, Wei Jiangong, Liang Jinqiang, et al. 2019. Complex gas hydrate system in a gas chimney, South China Sea. Marine and Petroleum Geology, 104: 29–39, doi: 10.1016/j.marpetgeo.2019.03.023
Yoo D G, Kang N K, Yi B Y, et al. 2013. Occurrence and seismic characteristics of gas hydrate in the Ulleung Basin, East Sea. Marine and Petroleum Geology, 47: 236–247, doi: 10.1016/j.marpetgeo.2013.07.001
Yuan Yusong, Zhu Weilin, Mi Lijun, et al. 2009. "Uniform geothermal gradient" and heat flow in the Qiongdongnan and Pearl River Mouth Basins of the South China Sea. Marine and Petroleum Geology, 26(7): 1152–1162, doi: 10.1016/j.marpetgeo.2008.08.008
Zhang Wei, Liang Jinqiang, Lu Jing'an, et al. 2017. Accumulation features and mechanisms of high saturation natural gas hydrate in

Shenhu Area, northern South China Sea. Petroleum Exploration and Development, 44(5): 708–719, doi: 10.1016/S1876-3804(17)30082-4

Zhang Wei, Liang Jinqiang, Su Pibo, et al. 2019. Distribution and characteristics of mud diapirs, gas chimneys, and bottom simulating reflectors associated with hydrocarbon migration and gas hydrate accumulation in the Qiongdongnan Basin, northern slope of the South China Sea. Geological Journal, 54(6): 3556–3573, doi: 10.1002/gj.3351

Zhang Gongcheng, Zeng Qingbo, Su Long, et al. 2016. Accumulation mechanism of LS 17-2 deep water giant gas field in Qiongdongnan Basin. Acta Petrolei Sinica (in Chinese), 37(S1): 34–46

Zhao Zhongxian, Sun Zhen, Wang Zhenfeng, et al. 2015. The high resolution sedimentary filling in Qiongdongnan Basin, Northern South China Sea. Marine Geology, 361: 11–24, doi: 10.1016/j.margeo.2015.01.002

Zhao Yanghui, Tong Dianjun, Song Ying, et al. 2016. Seismic reflection characteristics and evolution of intrusions in the Qiongdongnan Basin: Implications for the rifting of the South China Sea. Journal of Earth Science, 27(4): 642–653, doi: 10.1007/s12583-016-0708-2

Zhu Weilin, Huang Baojia, Mi Lijun, et al. 2009. Geochemistry, origin, and deep-water exploration potential of natural gases in the Pearl River Mouth and Qiongdongnan Basins, South China Sea. AAPG Bulletin, 93(6): 741–761, doi: 10.1306/02170908099